Determinants of synaptic integration and heterogeneity in rebound firing explored with data-driven models of deep cerebellar nucleus cells

Authors: Volker Steuber, Nathan W. Schultheiss, R. Angus Silver, Erik De Schutter, and Dieter Jaeger

Supplemental Materials

Detailed Description of Channel kinetics

All channel conductances G_j are modeled based on the Hodgkin & Huxley (1952) formalism and calculated as the product of a maximum conductance g_j and voltage or calcium dependent activation and inactivation variables m, h and z:

$$G_j = \bar{g}_j m^p h^q \quad \text{or} \quad G_j = \bar{g}_j z \qquad \text{(A1)}$$

The temporal evolution of all activation and inactivation variables x = {m, h, z} is determined by their steady state values x_∞ and their time constants τ_x:

$$\frac{dx}{dt} = \frac{x_\infty - x}{\tau_x} \qquad \text{(A2)}$$

For all voltage gated channels, the voltage dependences of the steady state activation and inactivation variables $x_\infty = \{m_\infty, h_\infty\}$ are represented by Boltzmann functions:

$$x_\infty = \frac{1}{1 + \exp\left(\frac{V - V_h}{k}\right)} \qquad \text{(A3)}$$

Where indicated, the time constants for activation and inactivation are described by:

$$\tau_x = \frac{A}{\exp\left(\frac{V - B}{C}\right) + \exp\left(\frac{V - D}{E}\right)} + F \qquad \text{(A4)}$$

All equations are for 32 ˚C.

Fast sodium current NaF

$$I_{NaF} = \bar{g}_{NaF}\, m^3 h\, (V - E_{Na})$$

with E_{Na} = 71 mV.

Activation m: V_h = -45 mV, k = -7.3 mV. The activation time constant τ_m is described by equation (A4), with A = 5.83 ms, B = 6.4 mV, C = -9 mV, D = -97 mV, E = 17 mV and F = 0.025 ms.

Inactivation h: V_h = -42 mV, k = 5.9 mV. The inactivation time constant τ_h also follows equation (A4), with A = 16.67 ms, B = 8.3 mV, C = -29 mV, D = -66 mV, E = 9 mV and F = 0.2 ms.

Persistent sodium current NaP

$$I_{NaP} = \bar{g}_{NaP}\, m^3 h\, (V - E_{Na})$$

with E_{Na} = 71 mV.

Activation m: V_h = -70 mV, k = -4.1 mV. The activation time constant is voltage independent and given by τ_m = 50 ms.

Inactivation h: V_h = -80 mV, k = 4 mV. The inactivation time constant is described by:

$$\tau_h = \frac{1750\, ms}{1 + \exp\left(\frac{V + 65\, mV}{-8\, mV}\right)} + 250\, ms$$

High voltage activated calcium current CaHVA

The current through high voltage activated calcium channels is modeled by the Goldman-Hodgkin-Katz equation:

$$I_{CaHVA} = \bar{p}_{CaHVA}\, m^3\, \frac{z^2 F^2 V}{RT}\, \frac{[Ca^{2+}]_i - [Ca^{2+}]_o \exp\left(\frac{-zFV}{RT}\right)}{1 - \exp\left(\frac{-zFV}{RT}\right)}$$

where p_{CaHVA} is the maximum Ca^{2+} permeability, z = 2 is the valency of Ca^{2+}, R = 8.3145 J K^{-1} mol^{-1} is the gas constant, F = 96480 C mol^{-1} is the Faraday constant and T is the thermodynamic temperature in K. The voltage dependence of the activation variable m is

described by a Boltzmann function (equation A3) with V_h = -34.5 mV and k = -9 mV, and the activation time constant is given by:

$$\tau_m = \frac{1ms}{31.746\left(\exp\left(\frac{V-5mV}{-13.89mV}\right)+1\right)^{-1} + 3.97\times10^{-4}mV^{-1}\left(V+8.9mV\right)\left(\exp\left(\frac{V+8.9mV}{5mV}\right)-1\right)^{-1}}$$

Low voltage activated calcium current CaLVA / CaT

$$I_{CaLVA} = \bar{g}_{CaLVA}\, m^2 h\,(V - E_{Ca})$$

with E_{Ca} = 139 mV.

Activation m: V_h = -56 mV, k = -6.2 mV. The activation time constant τ_m is described by equation (A4) with A = 0.333 ms, B = -131 mV, C = -16.7 mV, D = -15.8 mV, E = 18.2 mV and F = 0.204 ms.

Inactivation h: V_h = -80 mV, k = 4 mV. The inactivation time constant is given by

$$\tau_h = 0.333ms\exp\left(\frac{V+466mV}{66mV}\right) \qquad \text{for V < -81mV}$$

$$\tau_h = 0.333ms\exp\left(\frac{V+21mV}{-10.5mV}\right)+9.32\,ms \qquad \text{for V ≥ -81 mV}$$

Tonic non-specific cation current TNC

This is a mixed cation current with a with a reversal potential E_{TNC} = -35 mV and a voltage independent conductance:

$$I_{TNC} = \bar{g}_{TNC}\,(V - E_{TNC})$$

HCN current

$$I_h = \bar{g}_h\, m^2\,(V - E_h)$$

with E_h = -45 mV.

Activation m: V_h = -80 mV, k = 5 mV, τ_m = 400 ms.

Fast delayed rectifier fKdr

$$I_{fKdr} = \bar{g}_{fKdr}\, m^4 (V - E_K)$$

with E_K = -90 mV.

Activation m: V_h = -40 mV, k = -7.8 mV, τ_m given by equation (A4) with A = 13.9 ms, B = -40 mV, C = 12 mV, D = -40 mV, E = -13 mV, F = 0.1 ms.

Slow delayed rectifier sKdr

$$I_{sKdr} = \bar{g}_{sKdr}\, m^4 (V - E_K)$$

with E_K = -90 mV.

Activation m: V_h = -50 mV, k = -9.1 mV, τ_m given by equation (A4) with A = 14.95 ms, B = -50 mV, C = 21.74 mV, D = -50 mV, E = -13.91 mV, F = 0.05 ms.

Small conductance calcium dependent potassium current Sk

$$I_{Sk} = \bar{g}_{Sk}\, z (V - E_K)$$

with E_K = -90 mV.

The calcium dependent activation variable z is given by:

$$z_\infty = \frac{[Ca^{2+}]^4}{[Ca^{2+}]^4 + (3\times 10^{-4} mM)^4}$$

The calcium dependence of the activation time constant is described by:

$$\tau_z = \begin{cases} 60ms - 11.2\times 10^3\, ms\ mM^{-1}[Ca^{2+}] & for \quad [Ca^{2+}] < 0.005mM \\ 4ms & for \quad [Ca^{2+}] \geq 0.005mM \end{cases}$$

Calcium concentration

We assume that the Sk channel is selectively activated by calcium ions that enter the cell through CaHVA channels, and calculate the effective calcium concentrations using a simple phenomenological model:

$$\frac{d[Ca^{2+}]}{dt} = BI_{CaHVA} - \frac{[Ca^{2+}] - [Ca^{2+}]_{base}}{\tau_{Ca^{2+}}}$$

where $[Ca^{2+}]_{base}$ = 50 nM is the baseline calcium concentration, τ_{Ca2+} = 70 ms is the decay time constant and $B = k_{Ca2+}/v_{shell}$ is a free parameter that scales inversely with the volume of a hypothetical submembrane shell with a thickness of 200 nm. Tuning the model resulted in $k_{Ca2+} = 3.45 \times 10^{-7}$ mol C^{-1} in the soma and $k_{Ca2+} = 1.04 \times 10^{-6}$ mol C^{-1} in the dendritic compartments.

Detailed Description of Synaptic Properties

All synaptic conductances are described with double-exponential functions:

$$G_{syn}(t) = \frac{A g_{\max}}{\tau_{decay} - \tau_{rise}} \left(\exp(-t/\tau_{decay}) - \exp(-t/\tau_{rise}) \right)$$

where g_{max} is the maximum synaptic conductance, τ_{rise} and τ_{decay} are the rise and decay time constants, respectively, and A is a normalization factor chosen so that $G_{syn}(t)$ reaches a maximum value of g_{max}.

The total excitatory synaptic current comprises AMPA, fast NMDA and slow NMDA components and is given by:

$$I_{ex}(t) = \left(G_{AMPA}(t) + f_{fNMDA}(V) G_{fNMDA}(t) + f_{sNMDA}(V) G_{sNMDA}(t) \right)(V - E_{ex})$$

where E_{ex} = 0 is the excitatory reversal potential and f_{fNMDA} and f_{sNMDA} are factors describing the voltage dependence of the fast and slow NMDA conductances:

$$f(V) = \frac{1}{1 + p_1 \exp(-p_2 V)}$$

The parameters p_1 and p_2 are set to 0.002 and 0.109 mV^{-1} for the fast NMDA component and to 0.25 and 0.057 mV^{-1} for the slow NMDA component. The rise and decay time constants are 0.5 ms and 7.1 ms for AMPA, 5 ms and 20.2 ms for fast NMDA, and 5 ms and 136.4 ms for slow NMDA.

The GABAergic inhibitory synaptic current $I_{in}(t) = G_{GABA}(t)(V - E_{GABA})$ has rise and decay time constants of 0.93 ms and 13.6 ms and a reversal potential E_{GABA} between -70mV and -90mV.

Supplemental Figure 1.

Comparison between our standard model with a reduced number of synaptic inputs and a model that received synaptic inputs onto all dendritic compartments. In our standard model, 100 randomly chosen dendritic compartments were presented with 20 Hz random background excitation, and 400 randomly chosen dendritic compartments were presented with 30 Hz random background inhibition. In the fully connected model, all 485 dendritic compartments received random excitatory and inhibitory inputs with excitation and inhibition rates scaled to 4.12 and 24.74 Hz, respectively, in order to preserve the same total number of synaptic input rates as in the standard model. In both models, the somatic input rates were given by 50 times 20 Hz excitation and 50 times 30 Hz inhibition (see Methods). All simulations used a chloride reversal potential of -90 mV and unitary conductances of 50 pS for GABA, 100 pS for AMPA and 86 pS for NMDA (see Figure 10). **A,B.** Simulations of the standard model (top row) and the full synaptic model (bottom row) of Neuron 3. In **A** an intense inhibitory input burst (300 Hz) was added for a 250 ms period, resulting in a rebound after the offset of the inhibitory burst. **B** shows the ISI histograms for a period of 25 s before the inhibitory burst. Both the reduced and the full model fired spikes at very similar mean rates of 19.7 and 19.8 Hz, respectively. **C,D.** Simulations of Neuron 2 under the same conditions as for Neuron 3. Both the reduced and the full model fired at rates of 20.8 Hz.

Supplemental Figure 2.

A. Example of a recording, in which repetitive bursting was elicited at the offset of a hyperpolarizing current injection. This behavior was observed in 2 of 132 experiments. **B.** In the model repetitive bursting could be elicited when CaT was high, but both the HCN conductance and the NaP conductance were very low. This behavior was due to the hyperpolarization induced by SK current that without counteracting HCN and NaP currents led to sufficient hyperpolarization to deinactivate CaT current following a burst and thus allowed regenerative bursting. The SK current was activated by the inflow of

calcium during each burst regardless of whether HCN or NaP conductances were present. The lower trace shows that the addition of 2 S/m^2 HCN conductance eliminated repetitive bursting. This was due to HCN counteracting the SK current following the first burst of spiking, and thus not allowing the deinactivation of CaT, which would be necessary to trigger another burst.

Supplemental Figure 3.

The model as presented in the main manuscript was derived from kinetic descriptions of voltage-gated channels that were obtained by fitting published voltage-clamp data, primarily from Raman et al. (2000) [1]. For reasons that are not entirely clear these channel kinetics lead to a spike threshold that is about 10 mV hyperpolarized to the spike threshold found in our own current clamp data of DCN neurons even after subtracting a 10 mV junction potential. To examine whether this shift in potential had any effect on the findings reported in our study we created a 2nd model with adjusted channel parameters that led to a better phenomenological fit of our current clamp data but departed significantly from the published half activation and inactivation voltages of spike channels. In particular the following adjustments to channel kinetics were made to create the alternate model:

1) The activation and inactivation half-voltages of NaF, fKdr, sKdr, HCN, and CaHVA currents were shifted positive by 10 mV.
2) The voltage dependence of voltage-dependent time constants for NaF, fKdr, sKdr, HCN, and CaHVA currents was shifted positive by 10 mV.
3) The activation time constant of NaF was made voltage-independent and set to 0.025 ms.
4) A slow inactivation gate with a time constant of 70 ms at depolarized potentials was added to the NaF conductance. This follows recent results that slow inactivation is present in DCN neurons [2] and resulted in an improved fit with our current clamp data.
5) The NaP half-activation and inactivation voltage was shifted positive by 5 mV.

6) The NaP activation was sped up to a value of 0.3 ms at depolarized membrane potentials. This fast NaP activation is in better agreement with values in the literature than the previous value of 50 ms [3,4].

Panel A: A simulation with a 250ms negative current injection amplitude of -200 pA using the adjusted channel kinetics is shown. Note that the simulation trace is approximately 10 mV more depolarized than those of the base model (e.g. Figs. 1-2) without any significant alteration in spike shape, spontaneous spike frequency, and rebound components.
Panel B: Currents flowing through HCN, CaT and NaP rebound conductances during simulation shown in (A). Note that the NaP current in contrast to Fig. 4 now has a maximum as soon as the membrane potential depolarizes at the end of the current injection. Nevertheless, the contribution of NaP to the fast rebound is quite small, as the amplitude of CaT during the same time is several-fold higher. Also note that there is still a discernible pause between the fast and slow rebound components. This pause is due to the SK current activated by the calcium buildup occurring during the fast rebound spike burst.

The results from the adjusted channel kinetics demonstrate that the findings obtained with the base model are quite robust to minor adjustments of channel kinetics aimed to correct the noted hyperpolarized trajectory of the base model. Nevertheless we decided to keep the base model for the bulk of the results description, as the kinetics of the channels used were directly derived from the voltage-dependence measured in DCN neurons by Raman et al (2000).

Supplemental Figure 4

The synaptic parameters (AMPA and $GABA_A$ time constants and amplitudes) used in our base model were taken from our own work using dynamic clamping in DCN neurons [5]. However, more recent papers have presented updates on the kinetic parameters for AMPA and $GABA_A$ synapses onto DCN neurons [6-8]. To examine whether the

conclusions of our simulations depend on the synaptic parameters originally chosen we made an updated version of the model that included the following adjusted synaptic parameters based on results from the Raman group:

1) Rise and decay time constants of AMPA conductance were changed to 0.14 and 2.0 ms, respectively.
2) Rise and decay time constants of fast NMDA conductance were changed to 1.4 and 12.0 ms, respectively
3) Rise and decay time constants of fast NMDA conductance were changed to 1.4 and 40.0 ms, respectively
4) Rise and decay time constants of $GABA_A$ conductance were changed to 0.25 and 5.0 ms, respectively
5) The unitary synaptic maximal AMPA and $GABA_A$ conductances were increased to 1 nS and 2 nS, respectively.

Panel A: The changed synaptic input led to similar irregular spiking as the original synaptic parameters at a high conductance values (Fig 8C1). In this simulation, 485 AMPA/NMDA and 485 $GABA_A$ synapses were activated at mean rates of 14.3 and 22.9 Hz, respectively. The voltage-gated channel parameters are the same as shown in Supplemental Figure 3.

Panel B: The summed synaptic conductance traces during the simulation shown in (A). The total $GABA_A$ conductance exceeds the sum of AMPA and NMDA conductance. Nevertheless, this conductance combination speeds up spiking compared to spontaneous firing due to the much larger driving force of AMPA and NMDA conductance compared to the $GABA_A$ conductance. Also note that the fluctuations in $GABA_A$ conductance are larger than those in AMPA conductance, and that brief pauses in spiking are associated with transient increases in $GABA_A$ conductance.

Supplemental Figure 5.

Rebound in the presence of background synaptic input with adjusted model as demonstrated in Supplemental Figs. 3 and 4.

Panel A: The baseline rate of synaptic input here was 5 Hz for excitation and 7.5 Hz for inhibition. The level of rebound conductances present was 4 S/m^2 for NaP, 0.5 S/m^2 for HCN and 2.5 S/m^2 for CaT. The reversal potential for $GABA_A$ conductance was set to -80 mV. Despite substantial parameter changes in the simulation the rebound properties are very similar to the standard model (see Fig. 10), indicating that reported findings are robust against changing specific parameter settings.

Panel B: Ionic currents during baseline firing and rebound behavior. The fast rebound is supported by a CaT current that is not fully shunted even at this high level of GABA conductance. Although the induced NaP current is smaller than the baseline level of AMPA/NMDA current, it leads to a significant increase in spike frequency because it shifts the balance of inward and outward currents, which was close to a net current of zero without the added NaP current.

References cited in Supplemental Material:

1. Raman IM, Gustafson AE, Padgett D (2000) Ionic currents and spontaneous firing in neurons isolated from the cerebellar nuclei. J Neurosci 20: 9004-9016.
2. Aman TK, Raman IM (2007) Subunit dependence of Na channel slow inactivation and open channel block in cerebellar neurons. Biophysical Journal 92: 1938-1951.
3. Fleidervish IA, Gutnick MJ (1996) Kinetics of slow inactivation of persistent sodium current in layer V neurons of mouse neocortical slices. Journal of Neurophysiology 76: 2125-2130.
4. Baker MD, Bostock H (1997) Low-threshold, persistent sodium current in rat large dorsal root ganglion neurons in culture. Journal of Neurophysiology 77: 1503-1513.
5. Gauck V, Jaeger D (2003) The contribution of NMDA and AMPA conductances to the control of spiking in neurons of the deep cerebellar nuclei. J Neurosci 23: 8109-8118.
6. Telgkamp P, Padgett DE, Ledoux VA, Woolley CS, Raman IM (2004) Maintenance of high-frequency transmission at purkinje to cerebellar nuclear synapses by spillover from boutons with multiple release sites. Neuron 41: 113-126.
7. Pugh JR, Raman IM (2005) GABAA receptor kinetics in the cerebellar nuclei: evidence for detection of transmitter from distant release sites. Biophys J 88: 1740-1754.

8. Pugh JR, Raman IM (2006) Potentiation of mossy fiber EPSCs in the cerebellar nuclei by NMDA receptor activation followed by postinhibitory rebound current. Neuron 51: 113-123.

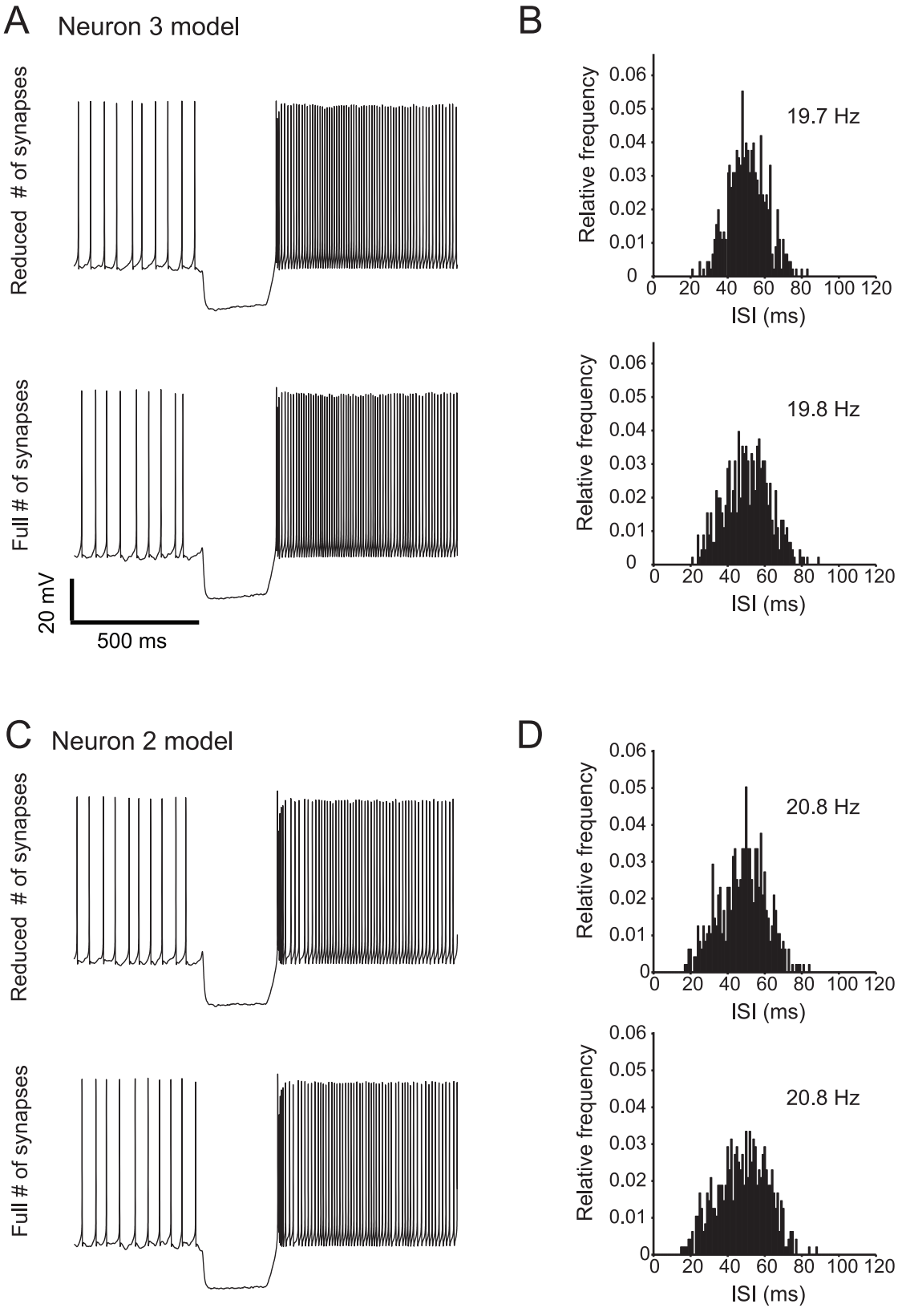

Supplementary Figure 1

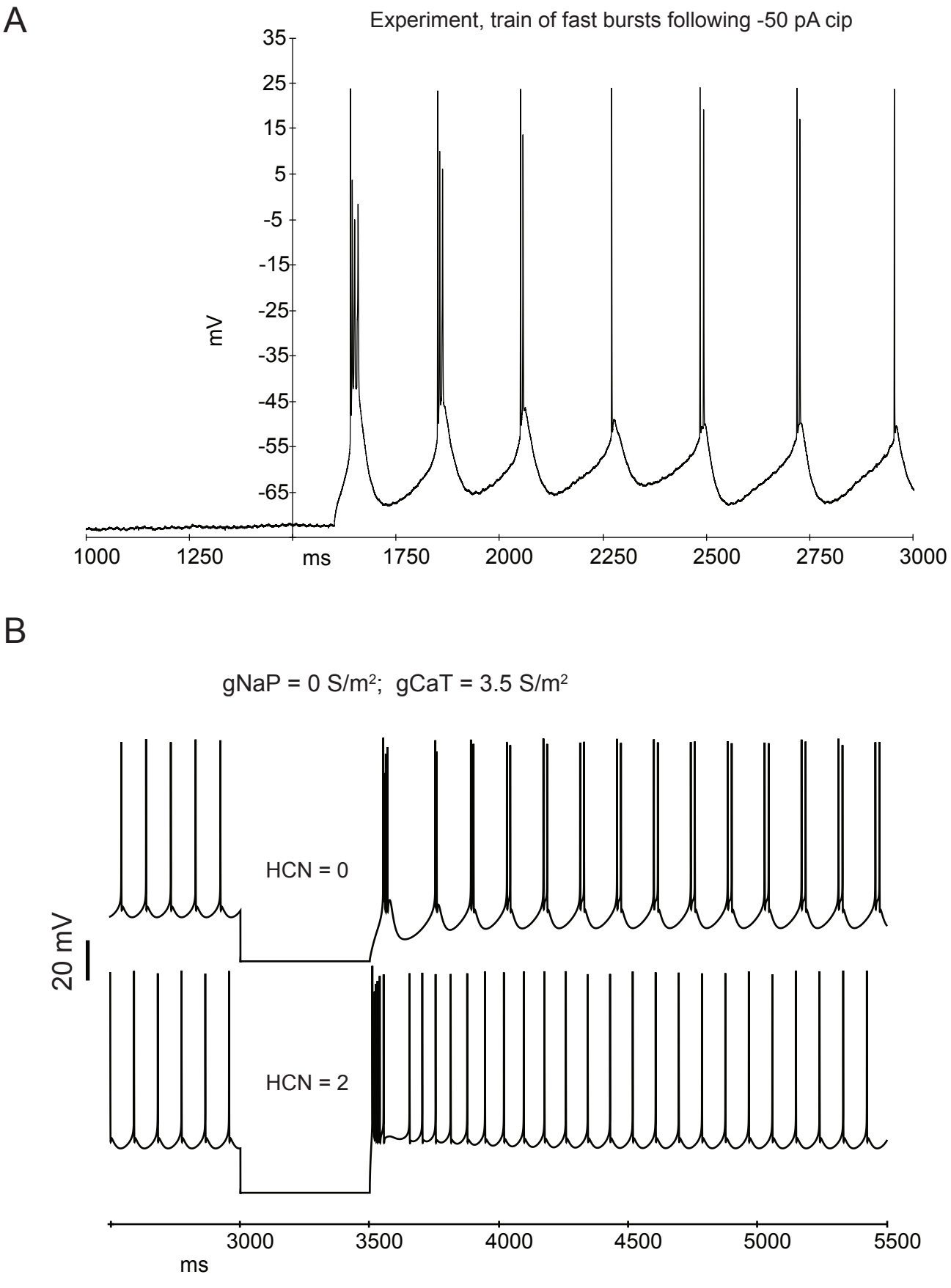

Supplementary Figure 2

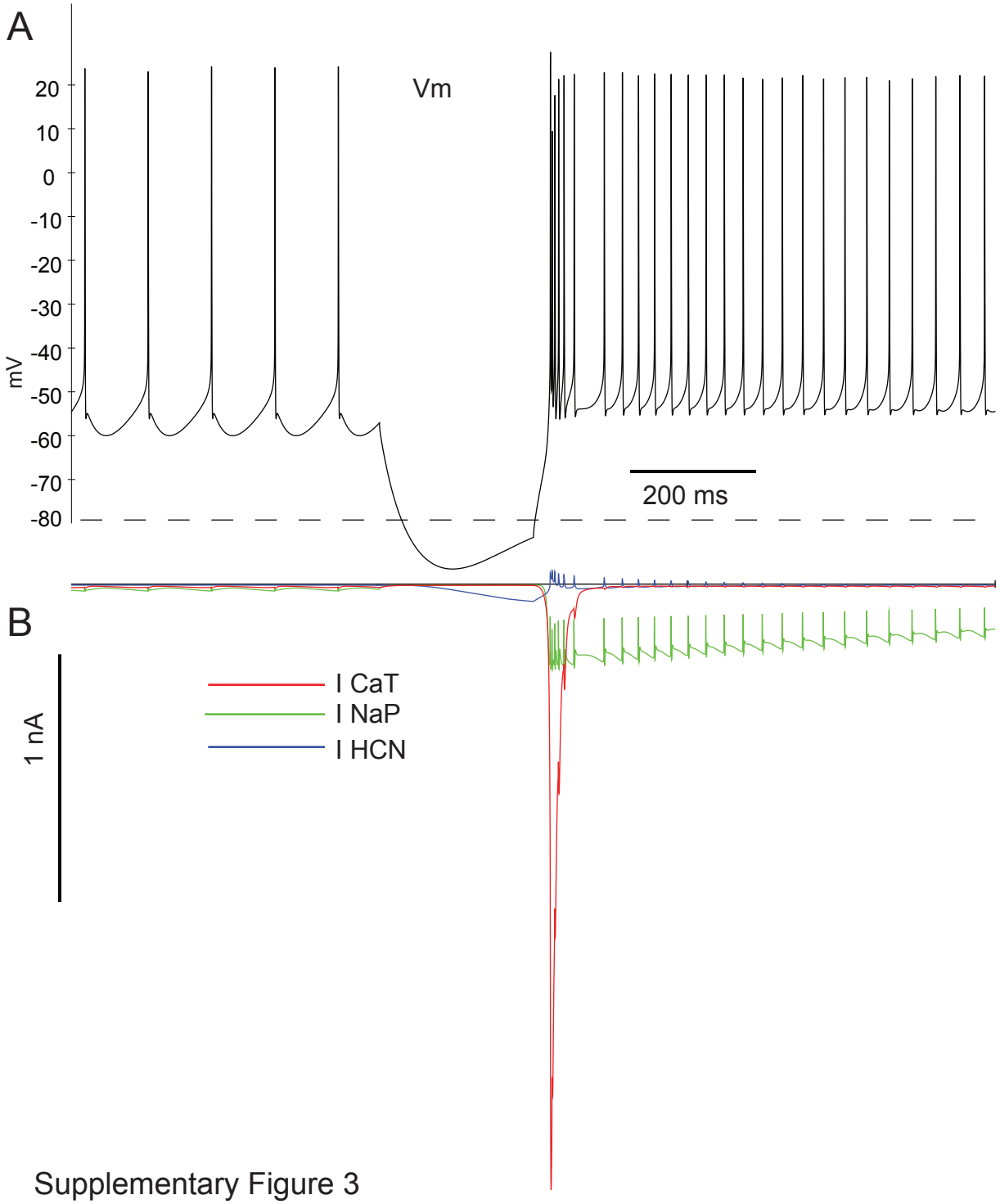

Supplementary Figure 3

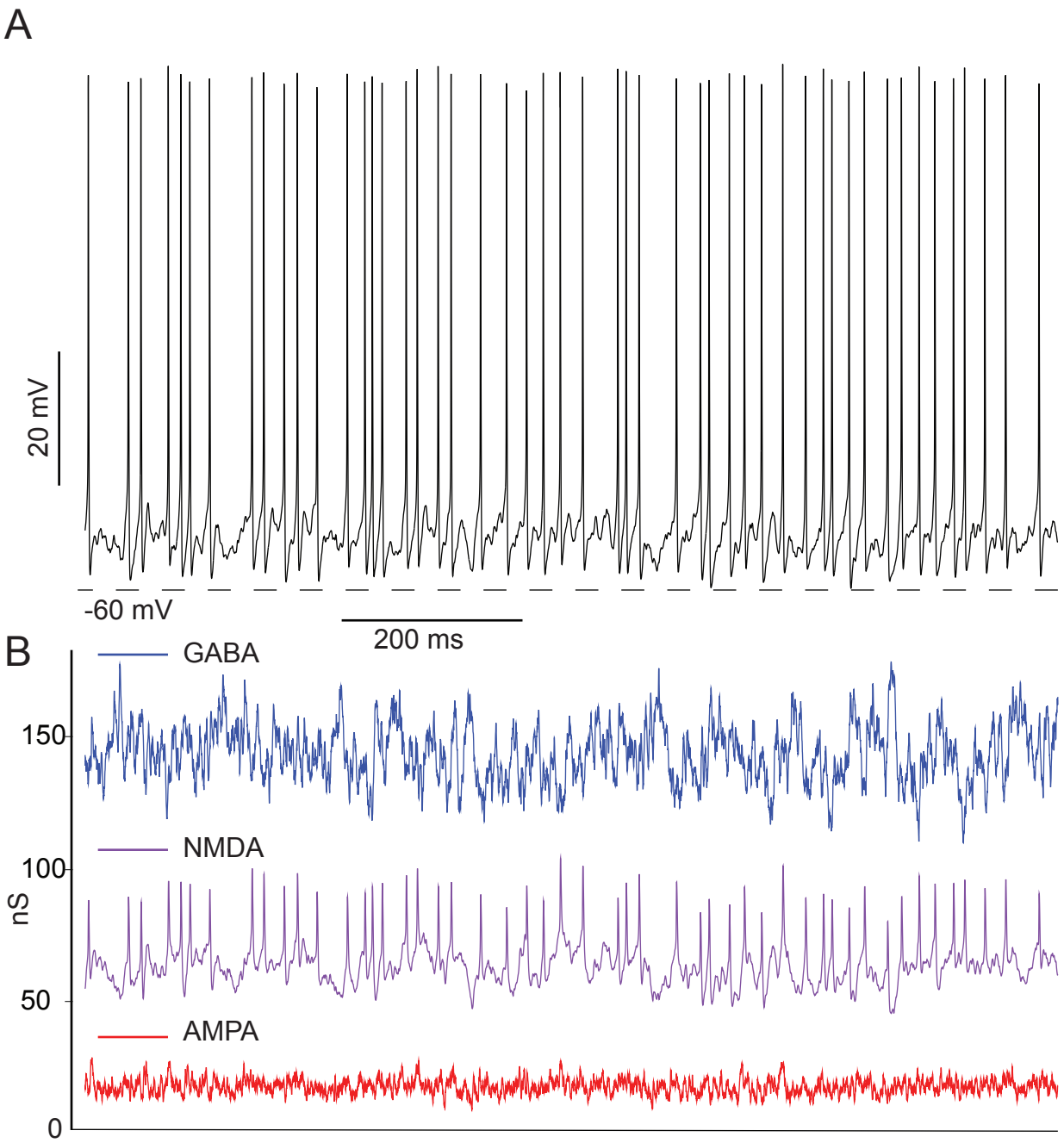

Supplementary Figure 4

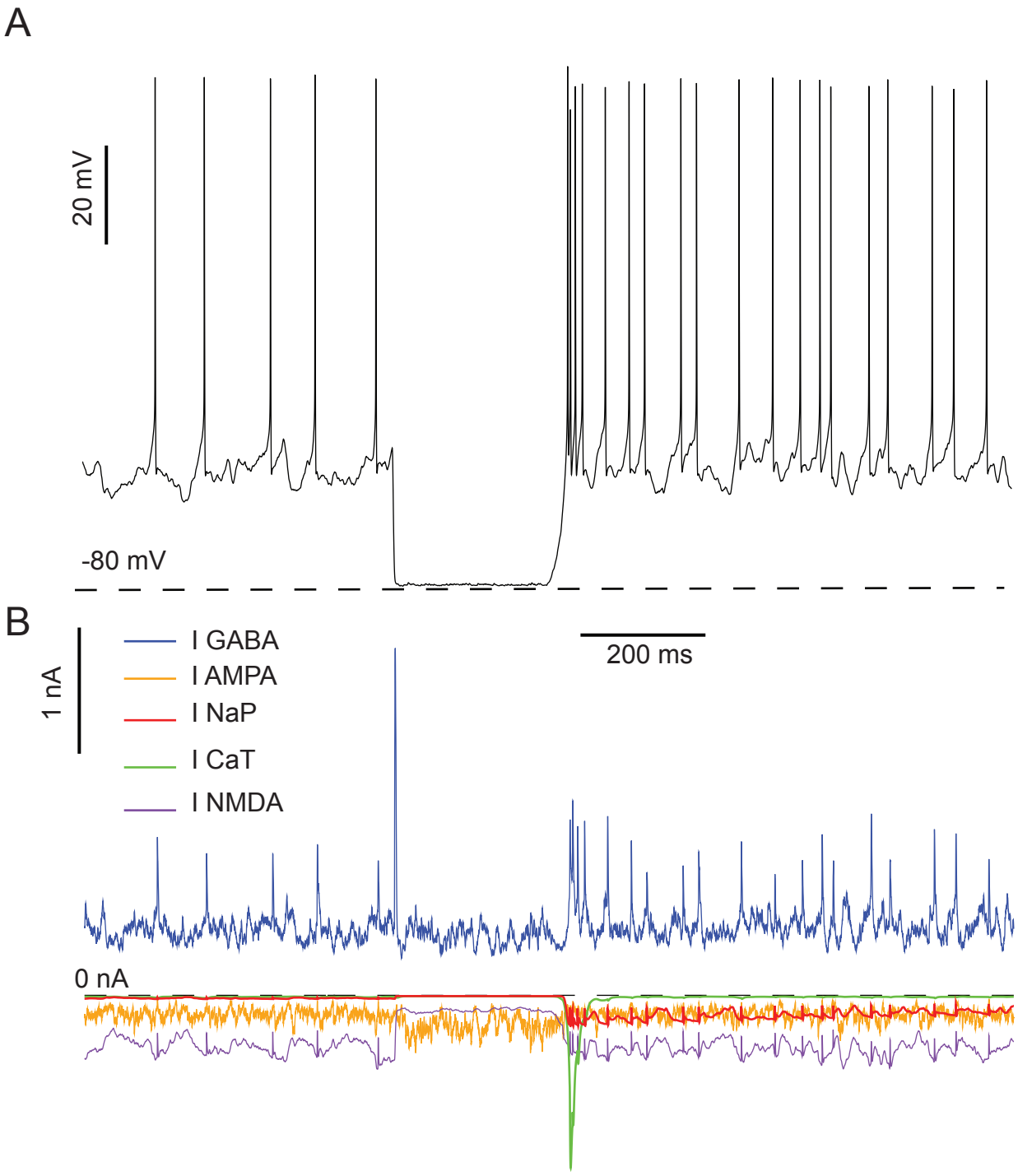

Supplementary Figure 5